Dual megathrust slip behaviors of the 2014 Iquique earthquake sequence

Author links open overlay panel LingsenMeng[a] HuiHuang[b] RolandBürgmann[c] Jean PaulAmpuero[d] AnneStrader[a]
Show more

https://doi.org/10.1016/j.epsl.2014.11.041

Highlights

- We analyzed the aseismic slow slip and the dynamic ruptures of the Iquique earthquake sequence.
- Repeater analysis of foreshocks favors independent slow slip event instead of cascade triggering.
- Mainshock back-projection reveals multiple episodes of re-ruptures of the foreshock zone.

Abstract

The transition between seismic rupture and aseismic creep is of central interest to better understand the mechanics of subduction processes. A Mw 8.2 earthquake occurred on April 1st, 2014 in the Iquique seismic gap of northern Chile. This event was preceded by a long foreshock sequence including a 2-week-long migration of seismicity initiated by a Mw 6.7 earthquake. Repeating earthquakes were found among the foreshock sequence that migrated towards the mainshock hypocenter, suggesting a large-scale slow-slip event on the megathrust preceding the mainshock. The variations of the recurrence times of the repeating earthquakes highlight the diverse seismic and aseismic slip behaviors on different megathrust segments. The repeaters that were active only before the mainshock recurred more often and were distributed in areas of substantial coseismic slip, while repeaters that occurred both before and after the mainshock were in the area complementary to the mainshock rupture. The spatiotemporal distribution of the repeating earthquakes illustrates the essential role of propagating aseismic slip leading up to the mainshock and illuminates the distribution of postseismic afterslip. Various finite fault models indicate that the largest coseismic slip generally occurred

down-dip from the foreshock activity and the mainshock hypocenter. Source imaging by teleseismic back-projection indicates an initial down-dip propagation stage followed by a rupture-expansion stage. In the first stage, the finite fault models show an emergent onset of moment rate at low frequency (<0.1Hz), while back-projection shows a steady increase of high frequency power (>0.5Hz). This indicates frequency-dependent manifestations of seismic radiation in the low-stress foreshock region. In the second stage, the rupture expands in rich bursts along the rim of a semi-elliptical region with episodes of re-ruptures, suggesting delayed failure of asperities. The high-frequency rupture remains within an area of local high trench-parallel gravity anomaly (TPGA), suggesting the presence of subducting seamounts that promote high-frequency generation. Our results highlight the complexity of the interactions between large-scale aseismic slow-slip and dynamic ruptures of megathrust earthquakes.

- **Previous** article in issue
- **Next** article in issue

Keywords

Chile
subduction
foreshock
slow slip
repeating earthquakes
back-projection

1. Introduction

The Chilean western coast is characterized by subduction of the Nazca plate underneath the South American plate, resulting in frequent, large interplate earthquakes. In the northern Chile subduction zone, the Nazca plate subducts east–northeast at a rate of ~67mm/yr(e.g., Métois et al., 2013) relative to the South American plate at a dip angle of 25°–30° (Chlieh et al., 2011).

On April 1st 2014, the Mw 8.2 Iquique subduction earthquake occurred approximately at a depth of 20.1 km, 50 km west of the northern Chilean coastline (Fig. 1, according to the catalog determined by the Centro Sismológico Nacional (CSN)). It has been long recognized that this region with high coupling rates (Chlieh et al., 2011, Métois et al., 2013), termed the “Iquique seismic gap” (Kelleher, 1972, Nishenko, 1985), had not experienced large earthquakes since a Mw 8.8 event in 1877 except for a Mw 7.4 event in 1967 and a Mw 7.7 earthquake in 2007 (Fig. 1-inset) (e.g., Comte and Pardo,

1991; Lomnitz, 2004; Peyrat et al., 2010). A Mw 8.6 earthquake occurred north of the Iquique gap in 1868, which was partially re-ruptured by the Mw 8.4 Arequipa earthquake in 2001. In 1995, a Mw 8.1 earthquake occurred just south of the Iquique gap in Antofagasta, rupturing a 180-km-long fault segment and causing surface deformation near the 2014 earthquake (Chlieh et al., 2004).

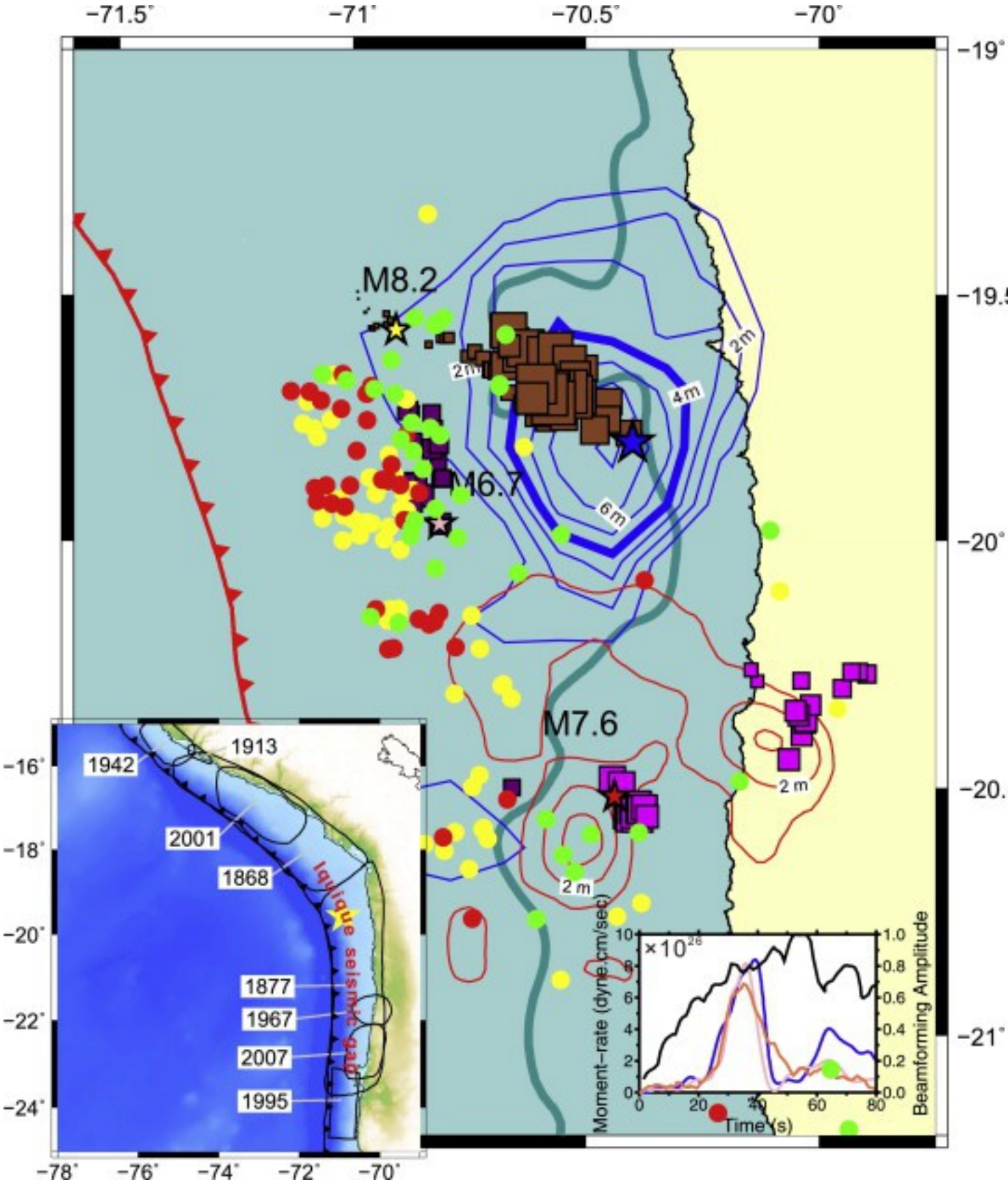
−71.5°
−71°
−70.5°
−70°
−19°
−19.5°
−20°
−20.5°
−21°
M8.2
M6.7
M7.6
2m
4m
6m
2 m
2 m
2 m
−16°
−18°
−20°
−22°
−24°
−78°
−76°
−74°
−72°
−70°
1913
1942
2001
1868
1877
1967
2007
1995
Iquique seismic gap
×10^26
Moment−rate (dyne.cm/sec)
Time (s)
Beamforming Amplitude

1. Download high-res image (875KB)
2. Download full-size image

Fig. 1. High-frequency back projections and average locations of repeating earthquake sequences or pairs. The blue contour lines denote the slip model (in cm) of the Mw 8.2 mainshock by Hayes et al. (2014) and the red contour lines denote the slip model of the Mw 7.6 aftershock (provided by Chen Ji). The purple, brown and magenta squares denote the back projections (0.5–2 Hz) of the Mw 6.7 foreshock, Mw 8.2 mainshock and Mw 7.6 aftershock, respectively, sized by the corresponding relative beamforming power. The thick dark green line denotes the contour of the Bouguer gravity anomaly of −10 mgals, with the anomaly increasing to the east. The green, red and yellow dots denote the average locations of repeating sequences containing events that occurred only before (preseismic-only), before and after (pre-and-post-seismic), and only after (postseismic-only) the Mw 8.2 event, respectively. The blue star denotes the best-fitting strong motion generation point (SMGP, Fig. 5). The left inset map shows historical rupture zones of several large earthquakes (closed curves) according to Chlieh et al., 2004, Chlieh et al., 2011and Peyrat et al. (2010). The location of Iquique seismic gap is approximately indicated. The yellow star denotes the Mw 8.2 hypocenter. The bottom-right inset shows the moment-rate functions of three finite-fault models (blue, pink and orange; same colors with contours, see also Fig. S1) and the beamforming amplitude of back-projection (black) of the Mw 8.2 mainshock as a function of time. (For interpretation of the references to color in this figure, the reader is referred to the web version of this article.)

The 2014 Mw 8.2 event was preceded by a vigorous foreshock sequence. The latest and most prominent foreshock sequence was initiated by the largest foreshock, a Mw 6.7 event on March 16th that may have occurred at 10 km depth in the overlying South America plate (Ruiz et al., 2014, Schurr et al., 2014). It then continued on the subduction thrust and migrated towards the mainshock hypocenter area, possibly accompanied by a large scale slow-slip event (Kato and Nakagawa, 2014, Ruiz et al., 2014), similar to the one preceding the 2011 Mw 9.0 Tohoku earthquake (Kato et al., 2012).

The Mw 8.2 event was also followed by an intensive aftershock sequence including a large Mw 7.6 on April 3rd that expanded the rupture zone to the south for a total length of about 200 km. Most aftershocks were located at the western and southern edges of the mainshock rupture zone.

The alternation between seismic rupture and aseismic creep is of central interest to better understand the mechanics of subduction processes (Hsu et al., 2003, Perfettini et al., 2005, Noda and Lapusta, 2013, Shirzaei et al., 2014). Here, we characterize the

Iquique earthquake sequence through repeating earthquake analysis, back-projection source imaging, finite-fault inversions and energy signatures of the local strong motion data. Our observations constitute a full spectrum of slip and open a window into the complexities of the dual slip behaviors on megathrust faults.

2. Slow pre- and postseismic slip inferred from repeating earthquakes

Repeating earthquakes found among the foreshocks and aftershocks can be used to illuminate aseismic slip (e.g., Igarashi et al., 2003). They are commonly interpreted as recurrent ruptures of asperities driven by surrounding aseismic slip (Nadeau and Johnson, 1998, Nadeau and McEvilly, 1999). Provided the asperities have a stationary seismic coupling and follow certain magnitude-slip scaling laws, the surrounding aseismic slip history can be tracked by the evolution of the cumulated seismic moment of repeating earthquakes (Igarashi et al., 2003). In this study we searched for repeating earthquakes in the proximity of the 2014 Iquique earthquake sequence.

The data processing and correlation analysis follow similar procedures to previous studies (e.g., Igarashi et al., 2003, Uchida and Matsuzawa, 2013). We converted the local magnitude (Ml) to moment magnitude (Mw) by combining Ml–Mw relations determined in northern Chile (Meneses, 2014) and in the 2010 Maule aftershock sequence (Lange et al., 2012):

$$Mw = 23Ml + 1.56 \quad \text{if} \quad Ml \leq 4.41$$

$$Mw = Ml + 0.09 \quad \text{if} \quad 4.41 < Ml < 5.71$$

We used event locations from the regional catalog ($Mw \geq 2.5$, from 1 January 2002 to 9 June 2014) determined by the CSN catalog. We only considered earthquakes with focal depths shallower than 80 km. Broadband seismograms recorded by 3 GSN stations and 20 IPOC stations were used (Fig. S2a). Although there were intermittent recording station failures, most events were simultaneously recorded by more than two stations (Fig. S3). The operation of the stations started at different times with most stations collecting data since 2006. For event pairs with hypocentral separations of less than 50 km, waveforms were windowed from 3 s before the theoretical P-wave arrival times to 10 s after the S-wave arrival to include enough S wave energy. Following Igarashi et al. (2003), the pass band was chosen according to the source size (inferred from magnitude) which is comparable to the quarter wavelength of the S-wave (at the cutoff frequency of the filter): 1–4 Hz for event pairs with both $Mw \geq 3$ or 1–8 Hz otherwise. If the cross-correlation coefficient (CC) exceeded 0.95 at two or more stations, the two events were classified into one group of repeating earthquakes (Fig. S4a). Then all groups with

common events were linked into a larger group until different groups were mutually exclusive (Fig. S4b).

We identified 147 repeating sequences of 343 events with CC>0.95 in the Mw range from 2.9 to 4.8 (among 3809 catalog events) (Figs. 1, S2). With a slightly lower threshold of CC>0.92, we found 223 sequences of 552 repeaters (Fig. S2). Previous work by Kato and Nakagawa (2014) found 12 repeating earthquake sequences with 26 events (Mw 2.4–4.6) between 1 January and 6 April 2014 in a reconstructed catalog by matched filter processing. By contrast, we identified more repeating earthquakes during this time period, although the CSN catalog is complete down to about Mw=3.5 from 2002 to the 1 April 2014 mainshock and to about Mw=4 after the mainshock (Fig. S5). This difference may be caused by the difference of event catalog and more strict criteria they used to define repeaters (longer correlation window from P arrival to 30 s after the S arrival and a correlation coefficient >0.95 at four or more stations). We also compared the fraction of repeaters as a function of time in the vicinity of the mainshock (region A) with that in an area to the south (region B) (Fig. S6a). As shown in Fig. S6b, the average fraction of repeaters in region A starts to increase since 2009 and is significantly larger (~15%) than that in region B in 2014 (~5%).

We estimated the cumulative slip of each repeating sequence based on the empirical relationship between fault slip d (cm) and seismic moment M0 (dyncm) developed by Nadeau and Johnson (1998) for repeating earthquakes in Parkfield, California:

$$\log(d) = -2.36 + 0.17 \log(M0)$$

This relationship has been applied in several repeating earthquake studies along the San Andreas fault system (Nadeau and McEvilly, 2004, Schmidt et al., 2005, Templeton et al., 2008), the Longitudinal Valley fault in Taiwan (Chen et al., 2008), and in the Japan subduction zone (Igarashi et al., 2003, Uchida et al., 2004). The relation between recurrence time, magnitude and creep rate found by Chen et al. (2007), unifying observations from three different regions, supports the applicability of Nadeau and Johnson's empirical relation to other regions. We note that dynamic rupture models of repeating earthquakes (Chen and Lapusta, 2009), consistent with the empirical relation by Nadeau and Johnson (1998), produce magnitude-independent stress drop. It is possible that some repeaters are missed by the analysis due to magnitude incompleteness and the slip estimates are uncertain. Nonetheless, they provide a first order quantification of the aseismic slip on the subduction thrust associated with interseismic creep, evolving foreshock activity, and postseismic afterslip.

According to the event occurrence times relative to the Mw 8.2 mainshock, we classified the repeating sequences into preseismic-only, postseismic-only and pre-and-

postseismic groups (shown in Fig. 1 and Fig. S2 by green, yellow and red dots, respectively). In general, the locations of preseismic-only repeaters surround the hypocenters of the Mw 6.7, Mw 7.6 and Mw 8.2 events and are downdip from the postseismic-only and pre-and-postseismic repeaters. The preseismic-only repeaters consist mostly of repeating pairs (except for two groups of three events) while the other two types of repeaters contain a large number of groups with three or more events (Figs. S7–S9), reflecting the larger amount of afterslip compared to preslip.

With CC>0.92 criterion, we identified thirteen groups of three or more repeaters in the pre-seismic-only repeaters. Nevertheless, the repeater analysis with the two thresholds (CC>0.92 and CC>0.95) produces the consistent spatial patterns (Fig. S2).

The along-strike positions of the foreshocks and repeaters are plotted against time in Fig. 2b. The seismicity rate increased abruptly after the Mw 6.7 event for approximately three days, possibly associated with the aftershock activity. Based on the shallow depth and diverse focal mechanisms of the Mw 6.7 event and many of its aftershocks, this initial burst may represent crustal events in the hanging wall (Ruiz et al., 2014). A second cluster of seismicity appeared six days later, further north and closer to the Mw 8.2 hypocenter. More repeating earthquakes are identified in this second sequence (Fig. 2b). The overall sequence migrated toward the hypocenter with a speed of about 3.6 km/day along the trench (or 5 km/day along the line joining the Mw 6.7 and Mw 8.2 epicenters, Yagi et al., 2014). The foreshock front approached the Mw 8.2 hypocenter, and then was followed by one week of significantly reduced seismicity before the mainshock nucleated.

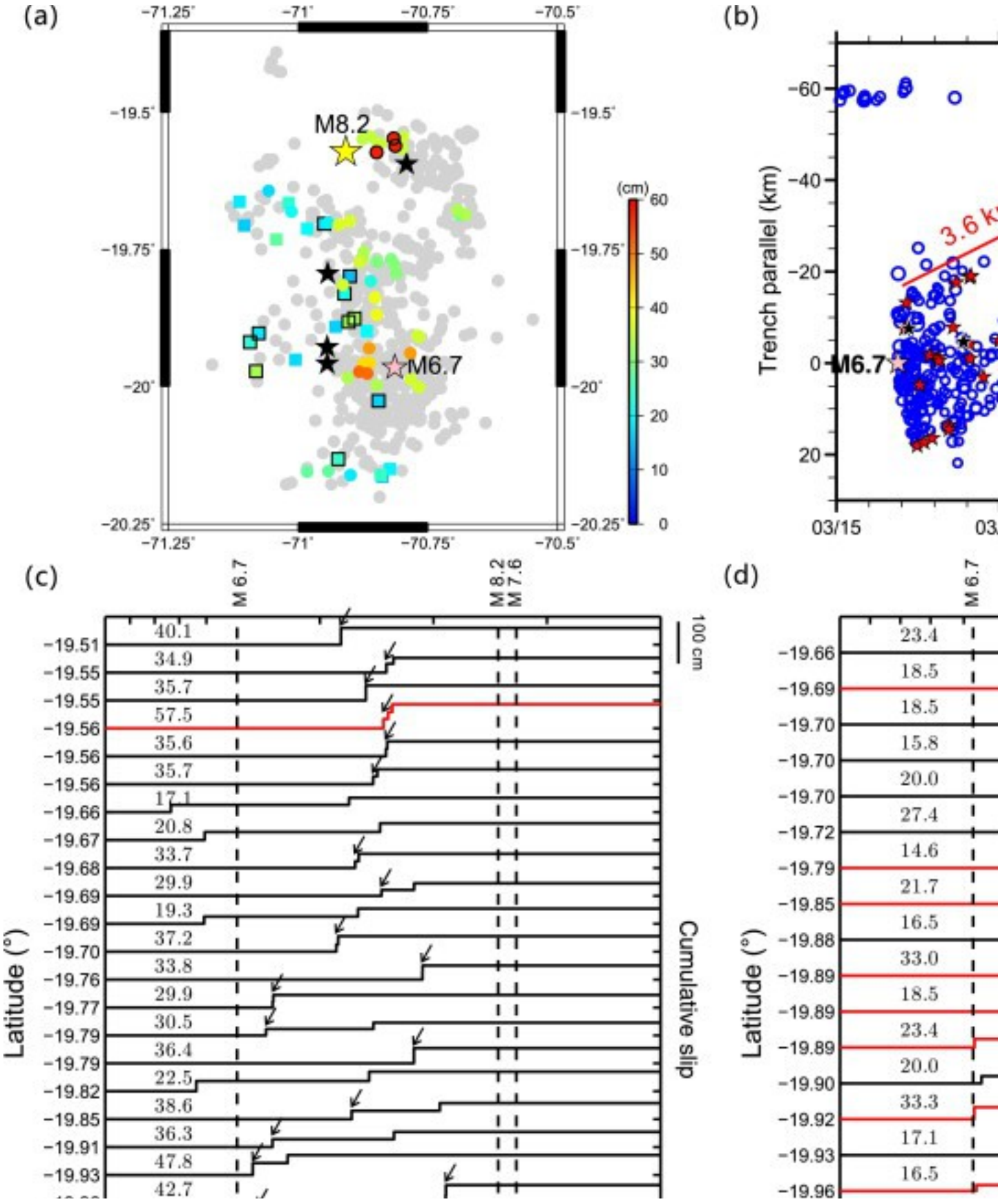
(a)
−71.25°
−71°
−70.75°
−70.5°
−19.5°
−19.75°
−20°
−20.25°
M8.2
M6.7
(cm)
60
50
40
30
20
10
0
(b)
Trench parallel (km)
−60
−40
−20
0
20
M6.7
3.6 k
03/15
03
(c)
M 6.7
M 8.2
M 7.6
100 cm
Latitude (°)
Cumulative slip
−19.51
−19.55
−19.55
−19.56
−19.56
−19.56
−19.66
−19.67
−19.68
−19.69
−19.69
−19.70
−19.76
−19.77
−19.79
−19.79
−19.82
−19.85
−19.91
−19.93
40.1
34.9
35.7
57.5
35.6
35.7
17.1
20.8
33.7
29.9
19.3
37.2
33.8
29.9
30.5
36.4
22.5
38.6
36.3
47.8
42.7
(d)
M 6.7
Latitude (°)
−19.66
−19.69
−19.70
−19.70
−19.70
−19.72
−19.79
−19.85
−19.88
−19.89
−19.89
−19.89
−19.90
−19.92
−19.93
−19.96
23.4
18.5
18.5
15.8
20.0
27.4
14.6
21.7
16.5
33.0
18.5
23.4
20.0
33.3
17.1
16.5

1. Download high-res image (1MB)
2. Download full-size image

Fig. 2. (a) The color circles and squares show the locations of the preseismic-only and pre-and-post-seismic repeating earthquakes. The symbol color indicates the cumulative slip of the corresponding repeating sequences during the foreshock period. Circles and squares with outlines indicate repeater groups with three or more events highlighted in (c) and (d), respectively. Gray dots show non-repeating shallow earthquakes (depth ≤ 80 km, Mw ≥ 2.5) during the foreshock period. Pink and yellow stars are the Mw 6.7 and Mw 8.2 events. (b) Migration of seismicity (blue circles) along the trench-parallel direction. Red and black stars show repeating events and large foreshocks (Mw ≥ 5.5), respectively. (c) and (d) show cumulative slip for the preseismic-only and pre-and-post-seismic sequences, respectively, arranged by their averaged latitude. The numbers on the lines indicate the amount of accumulated slip during the foreshock period. Repeater groups that contain more than two events during the foreshock period are marked with arrows. Note the change of time scale after 15 March 2014. (For interpretation of the references to color in this figure, the reader is referred to the web version of this article.)

Since the slow-slip behavior during the foreshock sequence is of particular interest, we focused on those repeating earthquake sequences containing events that occurred between the Mw 6.7 foreshock and the Mw 8.2 mainshock (the preseismic-only and pre-and-postseismic sequences shown in Fig. 2a). These sequences are located north of ~20.1S, in between the Mw 6.7 and Mw 8.2 epicenters. During the foreshock period, compared with the pre-and-postseismic repeaters, preseismic-only repeaters experienced shorter recurrence times (more of them occurred more than twice, Fig. 2c) and accumulated larger slip (~17.1–57.5cm, compared to ~14.6–33.3cm). The aseismic slip distribution during the foreshock period is obtained by averaging the cumulative slip of different groups (Fig. 3a). This pattern is compatible with that derived from GPS data by Ruiz et al. (2014). Based on the slip distribution we also obtained the total aseismic moment of 2.0872e+19Nm (grid size of 0.05×0.05°), which is close to the value of 4.4e+19Nm estimated by GPS data during the foreshock period. Note that the repeater-inferred moment depends on the area of the grid, although the estimates are on the same order within a reasonable range of grid sizes (Fig. S10). Another notable observation is that the onset time of the repeating earthquake sequences tends to be later further to the north (Figs. 2c and 2d), consistent with the general pattern of foreshock migration. It is notable that some preseismic-only repeaters occur very close to the Mw 8.2 epicenter (Fig. 2a).

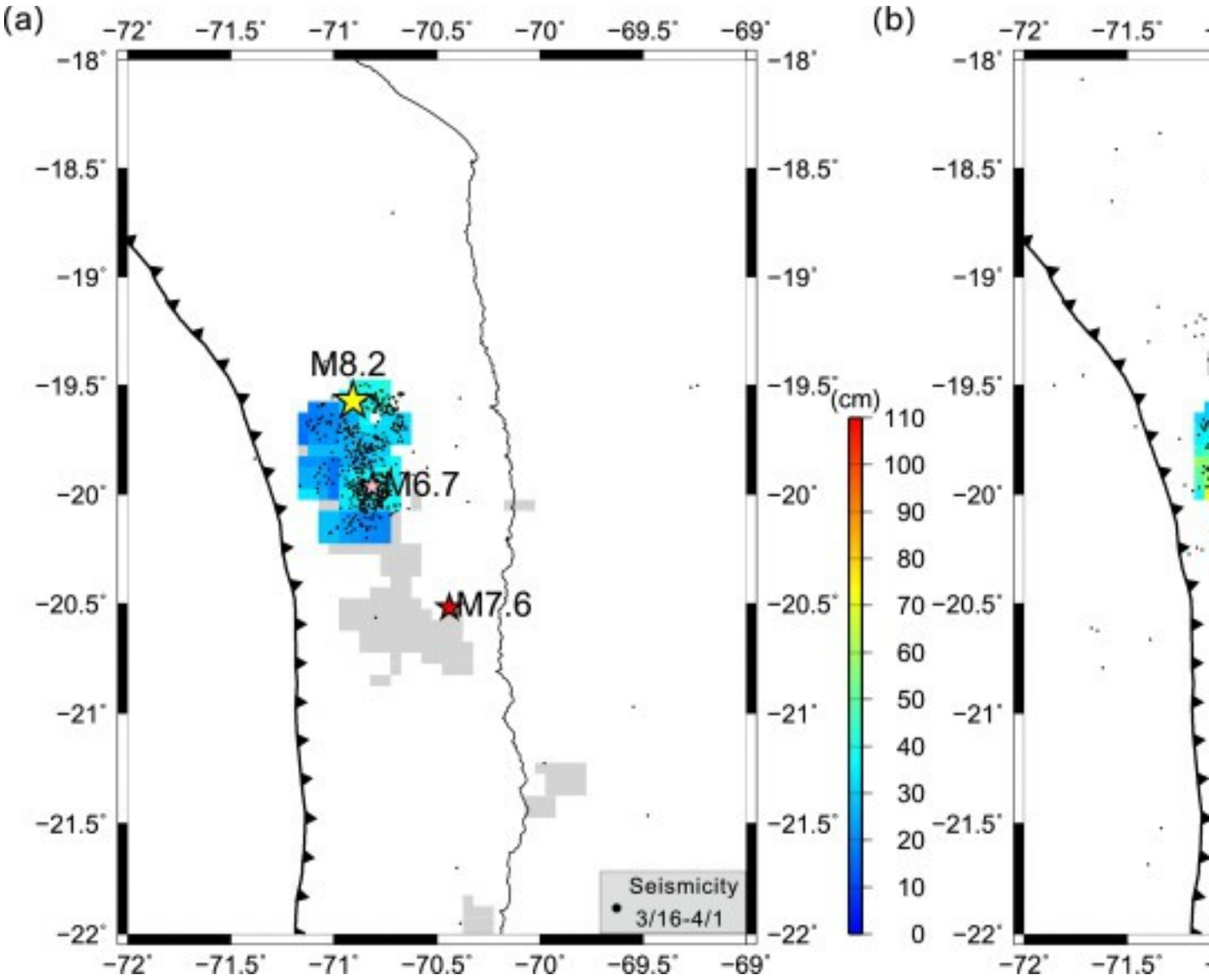

1. Download high-res image (569KB)
2. Download full-size image

Fig. 3. Averaged cumulative preseismic (a) and postseismic (b) slip distribution. The slip amounts (color boxes) estimated from the repeating earthquakes are averaged in 0.15 × 0.15° boxes shifted in 0.05° increments. Gray boxes indicate areas of repeaters that did not occur during the respective time period. The black dots show the foreshocks (a) and ∼2 months of aftershocks (b).

The pre-and-postseismic and postseismic-only repeaters illuminate the very early afterslip. After the occurrence of the Mw 8.2 mainshock, the repeaters are found in a much broader region updip of the rupture zone compared with those before the mainshock (Fig. 1). The afterslip is estimated by averaging the cumulative slip inferred from the postseismic repeating earthquakes. It is generally distributed in the updip

periphery of the preseismic and coseismic slip, although there is substantial overlap between the preseismic and postseismic slow slip zones (Figs. 3a and 3b).

3. Fast coseismic slip

The fast coseismic slip is effectively captured by low-frequency (LF) finite fault inversion and high-frequency (HF) back-projection. The focal mechanisms of the Mw 8.2 mainshock and Mw 7.6 aftershock were almost purely thrust and consistent with rupture on the plate interface, whereas the mechanism of the largest Mw 6.7 foreshock indicated rupture of a more westerly striking fault plane (Hayes et al., 2014). To extract the robust features of the coseismic slip behavior of the Mw 8.2 mainshock, we compared the coseismic slip distributions from several finite fault models based on teleseismic body and surface waveforms recorded by the global seismic network (GSN) (Fig. 1). Both the Hayes et al. model and the Caltech model are based on the finite fault inversion algorithm of Ji et al. (2002). The Yagi et al. model relies on a novel inversion approach accounting for the uncertainty of the Green's function (Yagi et al., 2014). The slip distributions of these models (Figs. 1, S1) vary due to intrinsic non-uniqueness of source inversions. Nevertheless, all models feature a predominant patch of large slip down-dip from the hypocenter. The slip extending to shallower depths close to the trench in the Caltech model is unlikely to be a robust feature, as it was not favored by tsunami data (Lay et al., 2014). The peak slip of the Hayes et al. model is ~8m located at ~19.75°S. Slip in the Caltech model is ~35kmfurther south and at greater depth. The Yagi et al. model is the shallowest, displaying peak slip to the south of the Hayes et al. model and the Caltech model, and is the smoothest of the three models. Common features include the spatial anti-correlation of the large coseismic slip with the foreshock sequence and the majority of repeating earthquakes. In particular, a robust observation is that the area of peak coseismic slip is devoid of repeating earthquakes. Interestingly, the preseismic-only repeaters are located closer to the coseismic slip than to the pre-and-postseismic and postseismic-only repeaters. Another common feature in all three models is the very slow initiation (Fig. 1-inset). The moment rate amplitude remains very low in the first 20 s, rapidly increasing afterwards. The slip model of the Mw 7.6 aftershock derived by Chen Ji from strong motion data indicates a rupture area extending southeast of the mainshock rupture, with two patches of slip to the east and southwest of its epicenter.

Back projection (BP) of HF seismic waves, aiming to map the source area generating strong seismic radiation, also provides crucial insights into the rupture process. The method is commonly applied to image earthquakes recorded at teleseismic distances

(e.g. Ishii et al., 2005), regional distances (Vallée et al., 2008; Meng et al., 2012b), and local distances (Fletcher et al., 2006; Meng et al., 2014a). The approach relies on only the timing information of coherent seismograms and is less affected by the uncertainty of seismic velocity models or the assumptions of fault kinematics. For the sake of waveform simplicity and coherency, BP typically requires seismograms recorded at teleseismic distances (between 30 to 90°). In the case of the Iquique earthquake, the only suitable large and dense teleseismic array is the USArray. Here we use USArray seismograms filtered between 2 s and 0.5 s (the highest band with adequate waveform coherency) to obtain a high-frequency image of the rupture process. Distinguishing from other BP studies of this earthquake (Lay et al., 2014, Schurr et al., 2014), we applied the Multitaper-MUSIC array processing technique (Meng et al., 2011, Meng et al., 2014b) with the "reference window" strategy (Meng et al., 2012a), which provides higher resolution than standard beamforming and mitigates the "swimming" artifact, a systematic drift of the HF energy towards the receiver array. The initial P-wave arrivals of the filtered waveforms are first aligned and are assumed to come from the hypocenter. The filtered seismograms are then back-projected onto the source region using differential travel times relative to the hypocentral travel time, based on the IASP91 velocity model. Since differential travel time is not sensitive to small source depth changes, we projected the BP images at a reference depth of 20 km. The BP, however, was sensitive to the choice of the epicenter. Here, we adopted the epicenter location of (−70.908,−19.572), determined by the CSN. The BP locations inherit a global uncertainty from the epicenter location uncertainty, likely less than the 10 km difference between the NEIC (−70.817,−19.642) and CSN epicenters. This difference might be accounted for by the uncertainty of the velocity model used to determine the epicenter locations and the use of more local stations in the CSN location.

One concern of the BP of the Iquique earthquake is the perturbation due to the depth phase *pP*. The azimuth of the USArray is close to the nodal plane of thrust events in South America, which leads to a significant depth phase in addition to the direct phase. This is demonstrated by the USArray waveforms and the *P* to *pP* ratio of a smaller M6.5 earthquake that occurred on November 13th, 2009 at a depth of 36 km (Figs. S11 and S12). Since our BP only assumes the direct phase, the depth phases result in a northward location bias towards the array, proportional to the source focal depth (Figs. S13 and S14). The BP of the relatively shallow Mw 6.7 foreshock at the depth of ~10km (Ruiz et al., 2014, Schurr et al., 2014) was not severely affected by the depth phase. However, the Mw 8.2 and Mw 7.6 earthquake ruptures reached deeper than 35 km; therefore, the bias of the BP caused by the depth phase may be larger than 30 km.

Nevertheless, since the source power is monotonically increasing in the first 55 s of the mainshock, the later and stronger direct phase suppresses the earlier depth phase. Therefore, the contamination by the depth phase should be minor up to the peak power. Our analysis suggests that the rupture process can be reliably imaged in the first 55 s of the mainshock and in the first 30 s of the Mw 7.6 aftershock.

The spatio-temporal history of the HF radiation of the Mw 8.2 mainshock is presented in Fig. 4. The extent of the HF rupture size was on the order of 40 km, rather compact compared with the slip distributions in finite fault models. The rupture speed was slow overall but highly variable. In this HF view, the earthquake comprised two distinct stages. It began with a down-dip propagation stage-1, following a linear path towards the southeast for 20 s (Fig. 4a). Stage-1 corresponds to the slow initiation phase in the finite fault models but, unlike the moment rate function, the BP power during the initial 20 s increased at constant rate and did not culminate in an abrupt change (black curve in Fig. 1-inset). The HF migration speed, estimated at 3 km/s (Fig. 4c), is not particularly slow. The HF rupture path followed the rim of the foreshock zone and coincided with the locations of a cluster of preseismic-only repeaters that failed previously in rapid succession. At the end of stage-1, the rupture reached the area of high coseismic slip of Hayes et al. model.

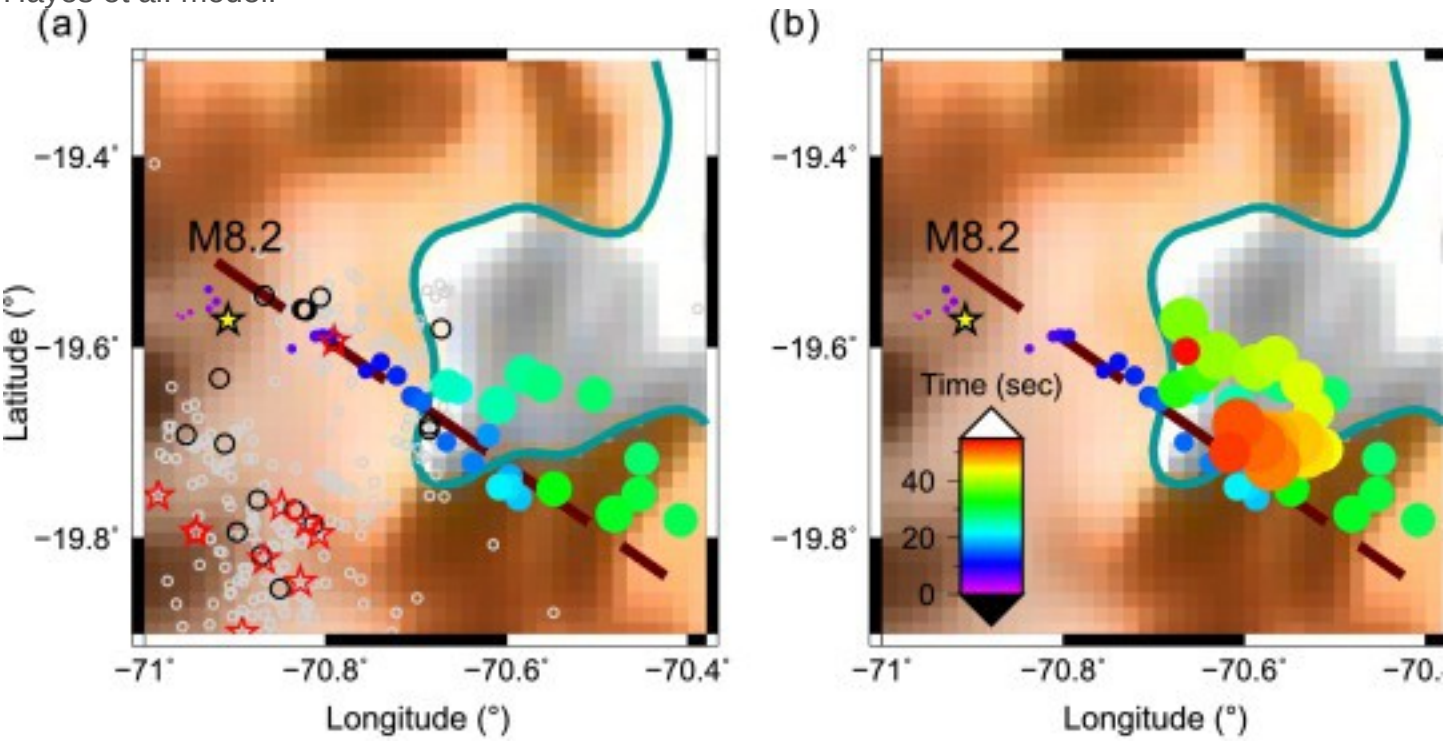

1. Download high-res image (589KB)
2. Download full-size image

Fig. 4. High frequency rupture process of the mainshock imaged by back-projection. The color circles are the back projections (0.5–2 Hz) of the mainshock from 0 to 33 s (a) and from 0 to 55 s (b). The color indicates rupture time and the size indicates the beamforming power. The open black circles in (a) show the locations of preseismic-only repeaters, part of which are along the path of the coseismic down-dip rupture. The gray open circles in (a) are all the foreshock locations and the open red stars are the Mw > 5 foreshocks. The background color denotes the gravity anomaly, with the area of anomaly greater than −10 mgals colored in white. (c) Timing of the BP radiators against their distance to the hypocenter projected on the direction of initial down-dip propagation (brown dashed line in (a) and (b)). The color denotes the distance normal to the projection line and the size indicates the power. The black dashed lines denote the boundaries of four different rupture stages. (For interpretation of the references to color in this figure, the reader is referred to the web version of this article.)

In the second stage, the HF radiation was confined in a small region north of the stage-1 HF rupture and followed a complex path with episodes of re-rupture. The rupture appeared as a rich, repeating sequence of bursts generated along the rim and at the center of a semi-elliptical region. We can decompose the HF radiation path during stage 2 into four sub-stages (2a to 2d). Between $t=22 \text{and} 30s$ (stage 2a), HF radiation propagates down-dip along an arcuate path that starts close to the stage-1 path and is centered roughly at the down-dip end of the stage-1 path (Fig. 4a). Near $t=30s$ (stage 2b), HF radiation migrates westward rapidly, approaching the down-dip end of stage-1 rupture. Subsequently, this rupture pattern appears to repeat. Until $t=45s$ (stage 2c), HF radiation migrates down-dip again, overlapping with the initial half of the stage-2a path, then bending south back to the stage-1 path (Fig. 4b). After $t=45s$ (stage 2d), HF radiation clusters again near the down-dip end of stage-1. Some details of these interpretations are subject to caution due to interference effects: sources that are separated in space and time may be artificially connected by our BP, which does not impose temporal sparsity of the sources. In particular, stages 2b and 2d could involve a jump of the HF radiation location instead of a continuous migration back to the center. It is also possible that the area involved in stages 2b and 2d was active during the whole stage 2 period, but was intermittently masked by the migrations during stages 2a and 2c. Nevertheless, two manifestations of re-rupture are robustly resolved: stages 2a and 2c unzip twice the arcuate rim of a semi-elliptical area, and stages 2b and 2d re-rupture areas involved in stage 1. Re-rupture in stage 2d is particularly well resolved owing to its higher HF radiation power than earlier stages. Also note that BP tracks the centroids of the HF radiation areas, but does not constrain their spatial extension at each time, hence the overlap between the areas of HF radiation during different sub-stages may be

more significant than depicted in Fig. 4. A compact HF rupture is consistently found in previous BP studies (Lay et al., 2014, Schurr et al., 2014). Our study, however, focused on the detailed spatiotemporal analysis of the rupture process. The re-rupture found here in stage 2 is also observed by Schurr et al. (2014). However, their results show re-rupture extending back to the hypocenter region, a feature inferred from analysis of waves arriving after the peak BP power which, as shown here, could be affected by the artifact caused by the depth phases.

The BP also revealed the rupture patterns of the Mw 7.6 aftershock and Mw 6.7 foreshock. The HF radiation of the Mw 7.6 aftershock was divided into two clusters at the down-dip edge of the two patches of slip (Fig. 1). The Mw 6.7 earthquake exhibited a unilateral northward propagation and its horizontal HF radiation seemed to coincide with locations of pre-seismic-only repeaters in the first burst of the foreshock sequence.

We inspected the near-source ground motions recorded by a strong motion network in Chile to identify the local signature of features we observed at teleseismic distances. We analyzed recordings of 19 surface accelerometers located along the western coast of northern Chile. We integrated to velocity and computed smoothed S wave energy envelopes. Fig. 5 shows 1–10 Hz envelopes sorted by station latitude. Amplitudes were normalized to emphasize the arrival-time moveout of the strong-motion phase. One prominent phase dominated the strong-motion records. The location and timing of the strong-motion-generation-point (SMGP) determined by grid search was 19.8S, 70.4W and 30 s after the mainshock origin time (blue star in Fig. 1 and Fig. 5), which is overall consistent with that of the Eastern-most HF spot imaged by BP (Fig. 4a). The residual between the predicted and observed arrival time was due to the limitation of the single point source assumption. For instance, the peak energy arrived later than predicted at the three southernmost stations, possibly due to a later rupture to the south (or early aftershock) affecting only the local stations. The fitting can probably be improved through finite fault models inverting the envelope of strong motion data (e.g. Nakahara, 2008), which is beyond the scope of this paper. Nevertheless, the location and timing of the most prominent burst is consistent with the deepest part of the down-dip HF propagation identified by BP.

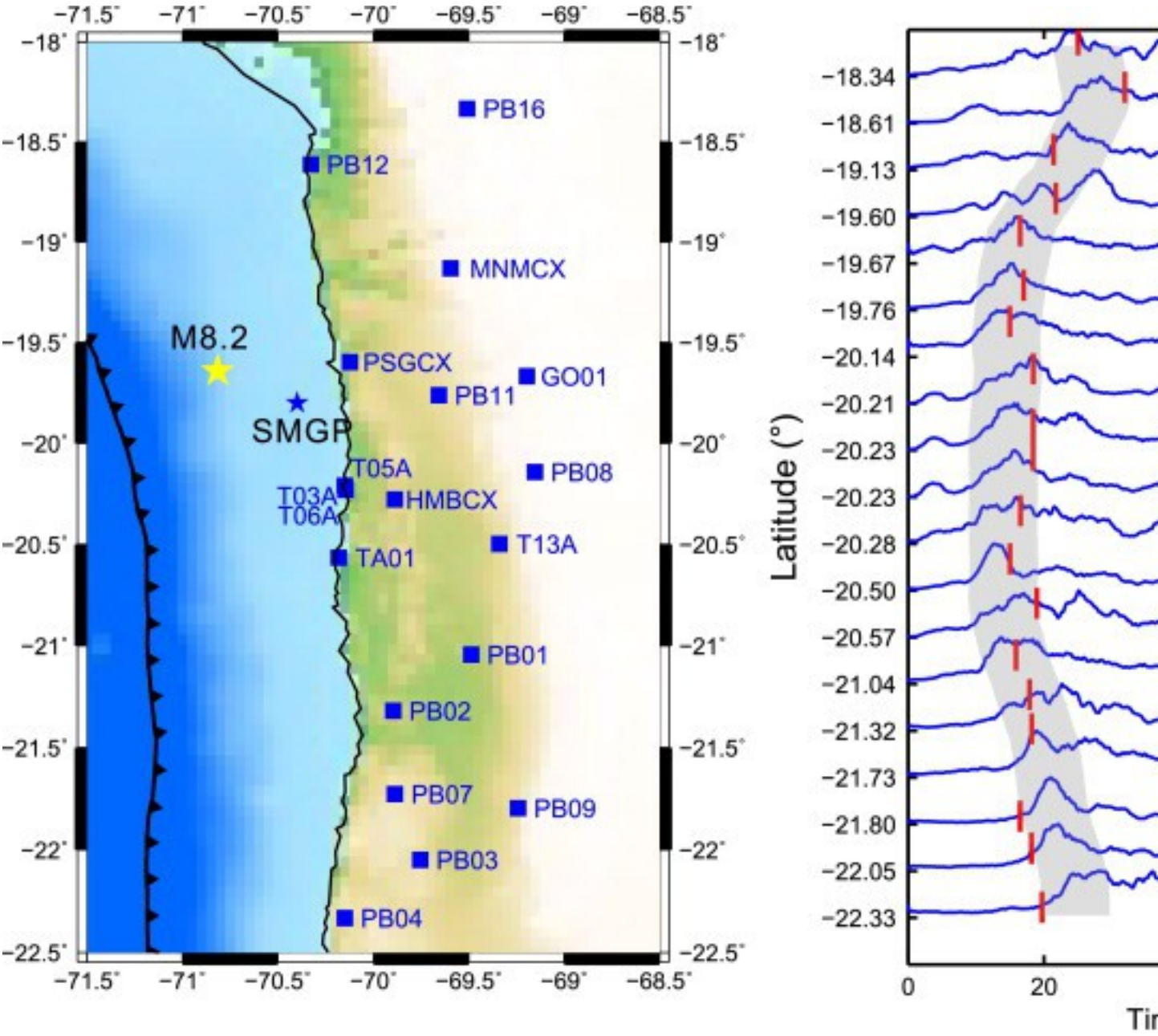

1. Download high-res image (954KB)
2. Download full-size image

Fig. 5. Smoothed energy envelopes of the E–W component of velocity waveforms (1–10 Hz) recorded by 19 strong-motion stations. The waveforms are aligned by the S-wave arrivals of the Mw 8.2 mainshock. The blue star denotes the best-fitting strong motion generation point (SMGP) (19.8S, 70.4W and ∼30 s after the origin time). The gray band and red ticks mark the observed and predicted timing of the peak energy. (For interpretation of the references to color in this figure, the reader is referred to the web version of this article.)

4. Discussion

The repeaters and back-projection analysis together with finite-slip models of the rupture provide an interesting opportunity to study the dual behavior of slip on megathrust faults. It has been long debated whether aseismic and seismic slips tend to occur on different sections of the plate interface or if they overlap substantially. Geodetic observations often suggested that postseismic afterslip occurred in places complementary to areas of large coseismic slip (e.g., Perfettini et al., 2005), although the poor resolution of off-shore slip by on-land geodesy challenges such inferences in subduction zones. Particularly, the geodetic observations are inconclusive regarding the contribution of slow slip preceding the Iquique earthquake (Schurr et al., 2014). The in situ repeating earthquakes help characterize the aseismic slip of megathrusts with better resolution (e.g., Uchida and Matsuzawa, 2013). Our observations of the Iquique earthquake sequence reveal a rather complicated relationship between the seismic and aseismic slip areas.

With the most strict criteria (CC>0.95), many of the identified repeaters are repeating pairs, especially before the mainshock. With a slightly lower threshold (CC>0.92), more groups with three or more events emerge (Figs. S7–S9). One might wonder if repeater pairs are truly diagnostic of aseismic slip, as “doublets” (neighboring earthquake pairs occurring within days to weeks) are not uncommon in catalogs. We find that some repeaters did occur before the 2014 sequence, which are most likely driven by the background aseismic slip. The scarcity of repeater sequences with three or more events occurring before the mainshock can be explained by the relatively small amount of total aseismic slip during the pre-seismic slow slip transient being insufficient to drive the repeater asperities to break more often. In comparison, many repeater sequences have more than two events after the mainshock, which is consistent with the total afterslip of the Mw 8.2 event being much larger than its preslip. Given our uniform and strict criteria, we consider both the repeating pairs and longer sequences as diagnostic of aseismic slip.

The contribution of aseismic creep is also supported by comparisons of the fraction of repeaters relative to the cumulative number of earthquakes (Fig. S6). The fraction increases significantly in the mainshock area but it remains almost constant in an area to the south. This increase of the repeater fraction is consistent with repeating earthquake sites located on the megathrust being triggered more efficiently by accelerating aseismic slip than by the background loading. Repeating earthquakes can result from a number of processes leading to accelerated loading rate or weakening,

including aseismic slip (on the same fault or on a neighboring fault), fluid flow or pressure transients, and stress transfer from neighboring earthquakes. The stress transfer mechanism would increase equally the number of repeaters and non-repeaters, which is not supported by our observation of elevated repeater fraction. We consider a fluid pressure transient mechanism to be unlikely if pressure transients are expected to migrate updip rather than along strike. The fact that the repeater fraction increases years before the 2014 sequence lends support to a multi-year gradual unlocking process proposed by Schurr et al. (2014).

The repeating earthquakes show a rather complex spatial distribution and do not simply reflect that of the overall foreshock and aftershock activities (Fig. S1). The aftershocks are distributed in the broad proximity of the Mw 8.2 mainshock, some of which overlap with the region of maximum slip. This region is however devoid of repeaters, suggesting full coupling and little postseismic slip. Alternatively, small asperities responsible for repeating earthquakes might be absent in the peak slip area of the mainshock. In the former scenario, our observations imply a purely stick-slip behavior. The spatial distribution of repeating earthquakes indicates a first order aseismic slip pattern, but their different temporal behaviors mark different degrees of seismic coupling, consistent with observations of the Tohoku-Oki earthquake (Uchida and Matsuzawa, 2013). The locations of preseismic-only repeaters (green in Fig. 1) overlap with areas of substantial coseismic slip, yet not the area of peak coseismic slip. This suggests that the periphery of the fully-locked asperity experienced both aseismic slip before the mainshock and coseismic slip (which shut off the repeaters). The pre-and-postseismic (red) and postseismic-only repeaters (yellow) suggest no (or smaller) coseismic slip and dominance of aseismic slip at the fringes of fully locked sections of the megathrust. The pre-and-postseismic repeaters (red) correspond to creeping areas experiencing large aseismic slip during the foreshock period, as well as post-earthquake afterslip (Figs. 2a and 2d). The areas of post-seismic-only repeaters (yellow) slipped too slowly during the foreshock sequence and temporarily accelerated during early afterslip. These could be creeping areas (interspersed by repeater patches) that were too stable to participate in the precursory slow slip event, but accelerated when triggered by the faster and larger stressing by the mainshock and its post-seismic slip. Alternatively, they could be locked regions that are also capable of aseismic slip, like the preseismic-only regions. Part of the preseismic-only and pre-and-post-seismic sequences (Fig. 2) experienced rapid recurrences during the foreshock period, which are mainly distributed along the path from the hypocenter of the Mw 6.7 foreshock to the Mw 8.2 mainshock. These asperities may have slipped slowly in prior years, then accelerated during the foreshock

sequence, and finally shut off temporarily by coseismic slip and stress drop (pre-seismic) or rapidly accelerated during afterslip (post-seismic). The pre-seismic repeater shutoff is either temporarily due to coseismic stress drop or permanently due to a change in fault zone properties induced by the rupture. In areas with no repeaters (e.g., the area of the large coseismic slip patch and some of the shallow and deep portions of the megathrust in Chile), no information is available on the mode and timing of slip. These areas could have been completely locked prior to the events or experienced aseismic slip.

Foreshock sequences accompanied by repeating earthquakes are thought to be a manifestation of a large-scale background slow slip transient (Brodsky and Lay, 2014, Kato et al., 2012, Uchida et al., 2004, Uchida and Matsuzawa, 2013). An alternative interpretation is that the migrating seismicity is simply produced by cascade triggering of a mainshock–aftershock sequence following Omori's Law (Helmstetter and Sornette, 2003), or through the drive of afterslip or the load by stress transfer from neighboring earthquakes or changes in fluid pore pressure. In this case the repeating earthquakes are driven by the afterslip of the moderate to large foreshocks instead of an independent slow slip event. In the 2014 Mw 8.2 Iquique earthquake sequence, we observed that some significant foreshocks ($Mw \geq 5.5$) were followed by the local burst-type repeaters (events with short reoccurrence times, less than 10 days) (Fig. 2a and Fig. S10), suggesting the contribution from afterslip events (Igarashi et al., 2003). However, the large-scale apparent foreshock migration speed is in favor of the independent slow-slip event (Kato et al., 2012). Furthermore, the repeaters are distributed in a wide area (~40×80km, Fig. 3a), difficult to be driven by only a few large foreshocks. The estimated repeater-inferred aseismic moment during the foreshock period is around 2.0872e+19Nm, consistent with the geodetic aseismic moment of 4.4e+19Nmduring the foreshock period (Ruiz et al., 2014). Both are of the same order with the total amount of seismic moment of all foreshocks (2.251e+19Nm). These comparisons again support the slow-slip model since the ratio of post-seismic to coseismic moment is generally small in most earthquakes.

Our results highlight the propagation of slow-slip preceding the Mw 8.2 Chile mainshock. The estimated migration speed of seismicity is ~3.6km/day. Although this speed is subjective to the choice of distance axis, our estimate is of the same order with that observed prior to the Tohoku-Oki earthquake (2–5 km/s) and the speed of the episodic slow-slip events in warm subduction zones such as Cascadia and Nankai (Kato et al., 2012). This is another piece of evidence supporting propagating slow-slip toward the mainshock hypocenter (Kato et al., 2012, Kato and Nakagawa, 2014).

Increased repeating earthquake activity has been observed in the foreshock sequences around the epicenters of some other large earthquakes such as the 1989 (Mw 7.1), the 1992 (Mw 6.9) and the 1994 (Mw 7.6) earthquakes off Sanriku, NE Japan (Uchida et al., 2004). Furthermore, our result reveals that the propagation of accelerated slow-slip is illuminated by the path of the preseismic-only repeaters (Figs. 2a and 2c). This indicates that the slow slip in the area of preseismic-only repeaters contributes more to the stress concentration around the Mw 8.2 epicenter, compared to the areas of other repeaters. The week of relative quiescence of seismicity preceding the Mw 8.2 event (Fig. 2b) is consistent with the nearly steady motion of GPS near the mainshock (Ruiz et al., 2014) and might correspond to a slow aseismic nucleation phase after the slow-slip transient ends.

The BP studies give rise to another interesting question in earthquake physics: what are the conditions for high frequency radiation? In several large megathrust earthquakes, including the Tohoku-Oki earthquake, the HF radiators identified by BP tended to be located down-dip from the LF slip of finite fault models (Meng et al., 2011; Yao et al., 2011, Lay et al., 2012). This was the case for the Mw 7.6 aftershock since the two HF groups were located near the downdip fringes of two LF slip patches. The SMGP of the Mw 8.2 mainshock, revealed by the strong motion envelope at even higher frequency, was also located deeper than the HF radiators in BP analysis. Our preferred interpretation of the HF radiators points to small-scale brittle asperities in the brittle–ductile transition zone, a highly heterogeneous region. The asperity model is similar to the current model explaining the repeaters (asperities loaded by surrounding aseismic slip). The similarity of the two models explains the colocation of the HF radiation in the initial stage of the Mw 8.2 mainshock and the HF radiation of the Mw 6.7 foreshock with the pre-seismic repeaters' rapid occurrence. However, complications from the Mw 8.2 mainshock HF radiation suggest that rheological heterogeneity is not the only contributor to HF radiation. The HF energy of the Mw 8.2 mainshock is north of the edge of large coseismic slip in some finite fault models, and certainly not at its down-dip edge. Furthermore, not all repeater/foreshock asperities generate HF radiation during the mainshock, suggesting a difference in the mechanics controlling the asperity of HF radiation and repeaters. Moreover, the mainshock HF radiation is confined in a relatively small region (~40km) given its magnitude. We observed connections between the gravity anomaly and coseismic rupture pattern. Fig. 6 shows the map of the trench-parallel gravity anomaly (TPGA), obtained by removing the effect of the trench-normal gravity gradient (Song and Simons, 2003). We found that the large coseismic slip (based on Hayes et al. model) is in a region of low TPGA, consistent with previous

findings that maximum coseismic moment release tends to occur in local TPGA minima or zones of negative TPGA (Loveless et al., 2010). The HF radiation is located on a TPGA peak, which may represent a geometrical barrier separating seismogenic segments. This feature may physically correspond to a subducting seamount that introduces geometrical heterogeneity on the megathrust and thus promotes strong HF radiation. Alternatively, the HF may occur as a result of dynamic triggering of adjacent fracture networks above the megathrust developed through the seamount subduction (Wang and Bilek, 2011). The incoming seamount chain in the TPGA map supports the possibility of seamount subduction. Fig. 6 shows that a scattered group of seamounts, located east of a more prominent seamount chain, may correspond to the region of HF radiation under the current direction of plate motion. This implies additional factors that control HF behavior, aside from rheological heterogeneity produced by along-dip material contrasts.

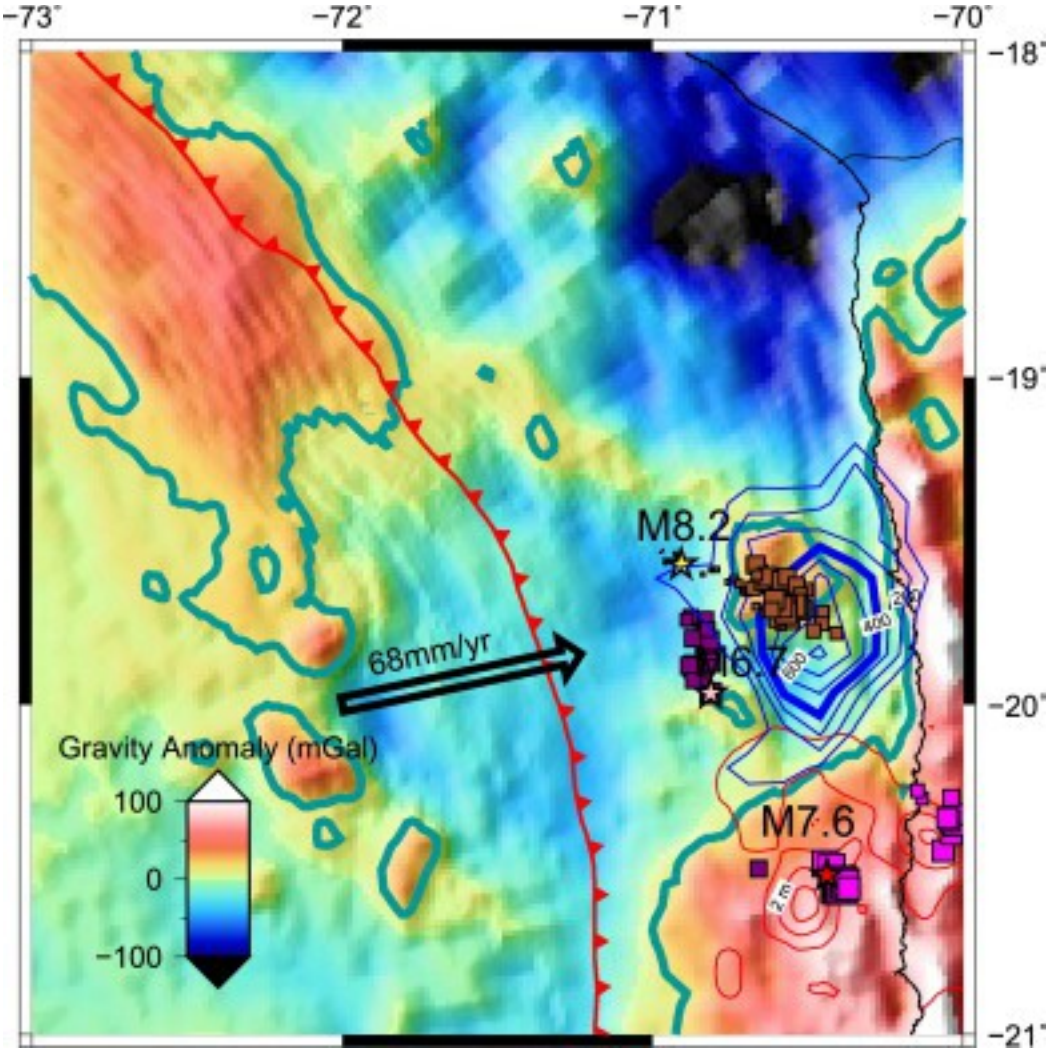

1. Download high-res image (782KB)

2. Download full-size image

Fig. 6. Trench-Parallel Gravity Anomaly (TPGA) in the study region. The thick dark green lines denote the TPGA contour of −10 mgals. The back projections (colored squares) and finite fault models (color contours) are denoted in the same fashion as in Fig. 1. The black arrow indicates the plate convergence between the Nazca and South America plates. (For interpretation of the references to color in this figure, the reader is referred to the web version of this article.)

The HF location coincides with a local gravity peak (gray area in Fig. 4a), which may represent a subducting seamount or an upper-crustal structure that concentrates stresses at its edges or increases normal stress on the megathrust. Alternatively, the HF radiation occurs as a result of dynamic triggering of crustal faults above the megathrust. Either of the two cases imply additional ingredients that control HF behavior, aside from rheological heterogeneity induced by the along-dip material contrast.

Another notable observation is the slow initiation of the Mw 8.2 mainshock. The finite-fault models show slow rise of the moment rate function during the first 20 s of the mainshock. The BP shows that the earthquake propagates down-dip through the northern fringe of the foreshock region. The stress in this area may have been kept at a low level by recurrent slow-slip events, which explains the deficiency of moment rate in a low-stress region. On the other hand, unlike the moment rate function, the HF power gradually increased because the LF is sensitive to slip while the HF power is sensitive to heterogeneity. The initial rupture nucleated within the low-stress region, resulting in low LF moment rate during the first 20 s. Nucleation zone expansion in the heterogeneous region increased HF energy much more efficiently than LF. In this particular case, the HF and LF observations show two different aspects of the nucleation process.

Repeated ruptures have been inferred from finite-fault source models of the Tohoku-Oki earthquake, either activated by the free-surface reflection from the trench (Ide et al., 2011) or as a second nucleation in the hypocenter region (Lee et al., 2011). In the stage-2 HF rupture of the Iquique earthquake, the rim and the center of a semi-elliptical region break twice, during stages 2a–2b and 2c–2d. A possible interpretation is that although the earthquake managed to nucleate and propagate down-dip through a cascading failure of small asperities in stage 1 and stage 2a, the low stress release was unable to break the larger asperities in the area. At the end of stage 2a, the down-dip rupture finally reached the deepest regions of higher stress accumulation. Subsequently, during stages 2b–2c–2d, the rupture transferred dynamic stress to

shallow depths and triggered asperities that remained unbroken along the circular rim. Such a hypothesis naturally explains the increasing HF power release towards later stages. A related model has been proposed for the 2011 Tohoku earthquake in which re-rupture is controlled by heterogeneities of initial stress and involves delayed ruptures and interaction between separate ruptures (Goto et al., 2012). Other possible re-rupture models involve stress concentration at the hypocenter of self-similar pulse-like ruptures (Nielsen and Madariaga, 2003, Gabriel et al., 2012) or a second stress drop induced by sudden fluid or gas pressurization due to dehydration or decarbonation transitions (O'Hara et al., 2006, Sulem and Famin, 2009, Brantut et al., 2010, Galvez et al., 2012). Stress transfer from the LF slip could also have contributed to re-rupturing asperities, but resolving this requires refined finite source inversions. The complicated HF rupture pattern imaged by BP might have affected the solutions of LF the Hayes et al. model and the Caltech model, in which each subfault is allowed to break only once. This observation demonstrates the challenge of formulating the source inversion problem to account for rupture complexity.

Acknowledgments

The IRIS (www.iris.edu) and GFZ (geofon.gfz-potsdam.de) data centers were used to access the broadband and strong-motion seismograms of the GSN (Global Seismic Network) and IPOC (Integrated Plate boundary Observatory Chile) network, respectively. The Chilean earthquake catalog was acquired from the Centro Sismologico Nacional (CSN). We thank Chen Ji for providing the slip model of the Mw 7.6 aftershock. We thank Jack Loveless for providing the Trench Parallel Gravity Anomaly (TPGA) code. The Global Marine Gravity Version 23.1 (http://topex.ucsd.edu/grav_outreach/) was used to compute the TPGA. We appreciate the valuable discussions with Chen Ji, Paul Davis, Yuji Yagi, An Yin, Javier Ruiz and Gilles Peltzer. H. Huang was supported by the National Natural Science Foundation of China (Grants: 41374048 and 41174038).

Appendix A. Supplementary material

The following is the Supplementary material related to this article.

Download Acrobat PDF file (10MB)Help with pdf files

MMC 1. This supplementary document contains the supporting figures for the back projection and repeating earthquake analysis of the 2014 Iquique earthquake sequence.

References

Brantut et al., 2010

N. Brantut, A. Schubnel, J. Corvisier, J. Sarout**Thermochemical pressurization of faults during coseismic slip**

J. Geophys. Res., 115 (2010), p. B05314, 10.1029/2009JB006533

Brodsky and Lay, 2014

E.E. Brodsky, T. Lay**Recognizing foreshocks from the 1 April 2014 Chile earthquake**

Science, 344 (2014), pp. 700-702

CrossRefView Record in Scopus

Chen et al., 2007

K.H. Chen, R.M. Nadeau, R.-J. Rau**Towards a universal rule on the recurrence interval scaling of repeating earthquakes?**

Geophys. Res. Lett., 34 (2007), p. L16308

Chen et al., 2008

K.H. Chen, R.M. Nadeau, R.-J. Rau**Characteristic repeating earthquakes in an arc-continent collision boundary zone: the Chihshang fault of eastern Taiwan**

Earth Planet. Sci. Lett., 276 (2008), pp. 262-272

ArticleDownload PDFView Record in Scopus

Chen and Lapusta, 2009

T. Chen, N. Lapusta**Scaling of small repeating earthquakes explained by interaction of seismic and aseismic slip in a rate and state fault model**

J. Geophys. Res., Solid Earth (1978–2012), 114 (B1) (2009)

Chlieh et al., 2004

M. Chlieh, J.B. De Chabalier, J.C. Ruegg, R. Armijo, R. Dmowska, J. Campos, K.L. Feigl**Crustal deformation and fault slip during the seismic cycle in the North Chile subduction zone, from GPS and InSAR observations**

Geophys. J. Int., 158 (2004), pp. 695-711

CrossRefView Record in Scopus

Chlieh et al., 2011

M. Chlieh, H. Perfettini, H. Tavera, J.-P. Avouac, D. Remy, J.-M. Nocquet, F. Rolandone, F.Bondoux, G. Gabalda, S. Bonvalot**Interseismic coupling and seismic potential along the Central Andes subduction zone**

J. Geophys. Res., 116 (2011), p. B12405

Comte and Pardo, 1991

D. Comte, M. Pardo**Reappraisal of great historical earthquakes in the northern Chile and southern Peru seismic gaps**

Nat. Hazards, 4 (1991), pp. 23-44

CrossRefView Record in Scopus

Fletcher et al., 2006

J.B. Fletcher, P. Spudich, L.M. Baker**Rupture propagation of the 2004 Parkfield, California, earthquake from observations at the UPSAR**
Bull. Seismolog. Soc. Am., 96 (4B) (2006), pp. S129-S142
CrossRefView Record in Scopus

Gabriel et al., 2012

A. Gabriel, J.-P. Ampuero, L.A. Dalguer, P.M. Mai**The transition of dynamic rupture styles in elastic media under velocity-weakening friction**
J. Geophys. Res., 117 (2012), p. B09311, 10.1029/2012JB009468

Galvez et al., 2012

P. Galvez, L.A. Dalguer, J.-P. Ampuero**Modeling dynamic source rupture with slip reactivation and near-source ground motion of the 2012 Mw 9.0 Tohoku earthquake**
Abstract S33A-2516 presented at
2012 Fall Meeting, AGU, San Francisco, CA, 3–7 December (2012)

Goto et al., 2012

H. Goto, Y. Yamamoto, S. Kita**Dynamic rupture simulation of the 2011 off the Pacific coast of Tohoku earthquake: multi-event generation within dozens of seconds**
Earth Planets Space, 64 (12) (2012), pp. 1167-1175
CrossRefView Record in Scopus

Hayes et al., 2014

G.P. Hayes, M.W. Herman, W.D. Barnhart, K.P. Furlong, S. Riquelme, H.M. Benz, E.Bergman, S. Barrientos, P.S. Earle, S. Samsonov**Continuing megathrust earthquake potential in Chile after the 2014 Iquique earthquake**
Nature, 512 (2014), pp. 295-298
CrossRefView Record in Scopus

Helmstetter-

and Sornette, 2003

A. Helmstetter, D. Sornette**Foreshocks explained by cascades of triggered seismicity**
J. Geophys. Res., 108 (2003), p. 2457
View Record in Scopus

Hsu et al., 2003

Y.-J. Hsu, M. Simons, S.-B. Yu, L.-C. Kuo, H.-Y. Chen**A two-dimensional dislocation model for interseismic deformation of the Taiwan mountain belt**
Earth Planet. Sci. Lett., 211 (2003), pp. 287-294
ArticleDownload PDFView Record in Scopus

Ide et al., 2011

S. Ide, A. Baltay, G.C. Beroza**Shallow dynamic overshoot and energetic deep rupture in the 2011 Mw 9.0 Tohoku-Oki earthquake**
Science, 332 (2011), pp. 1426-1429
CrossRefView Record in Scopus

Igarashi et al., 2

T. Igarashi, T. Matsuzawa, A. Hasegawa**Repeating earthquakes and interplate aseismic slip in the northeastern Japan subduction zone**
J. Geophys. Res., 108 (2003), p. 2249

Ishii et al., 2005

M. Ishii, P.M. Shearer, H. Houston, J.E. Vidale**Extent, duration and speed of the 2004 Sumatra–Andaman earthquake imaged by the Hi-Net array**
Nature, 435 (7044) (2005), pp. 933-936
CrossRefView Record in Scopus

Ji et al., 2002

C. Ji, D.J. Wald, D.V. Helmberger**Source description of the 1999 Hector Mine, California, earthquake, Part I: Wavelet domain inversion theory and resolution analysis**
Bull. Seismol. Soc. Am., 92 (2002), pp. 1192-1207
CrossRefView Record in Scopus

Kato and Nakaga

A. Kato, S. Nakagawa**Multiple slow-slip events during a foreshock sequence of the 2014 Iquique, Chile Mw 8.1 earthquake**
Geophys. Res. Lett, 41 (15) (2014), pp. 5420-5427, 10.1002/2014GL061138
CrossRefView Record in Scopus

Kato et al., 2012

A. Kato, K. Obara, T. Igarashi, H. Tsuruoka, S. Nakagawa, N. Hirata**Propagation of slow slip leading up to the 2011 Mw 9.0 Tohoku-Oki earthquake**
Science, 335 (2012), pp. 705-708
CrossRefView Record in Scopus

Kelleher, 1972

J.A. Kelleher**Rupture zones of large South American earthquakes and some predictions**
J. Geophys. Res., 77 (1972), pp. 2087-2103
CrossRef

Lange et al., 201

D. Lange, F. Tilmann, S.E. Barrientos, E. Contreras-Reyes, P. Methe, M. Moreno, B. Heit, H.Agurto, P. Bernard, J.-P. Vilotte, S. Beck**Aftershock seismicity of the 27 February 2010 Mw 8.8 Maule earthquake rupture zone**
Earth Planet. Sci. Lett., 317–318 (2012), pp. 413-425
ArticleDownload PDFView Record in Scopus

Lay et al., 2012

T. Lay, H. Kanamori, C.J. Ammon, K.D. Koper, A.R. Hutko, L. Ye, H. Yue, T.M. Rushing**Depth-varying rupture properties of subduction zone megathrust faults**
J. Geophys. Res., 117 (2012), p. B04311, 10.1029/2011JB009133

Lay et al., 2014

T. Lay, H. Yue, E.E. Brodsky, C. An**The 1 April 2014 Iquique, Chile, Mw 8.1 earthquake rupture sequence**
Geophys. Res. Lett., 41 (2014), 10.1002/2014GL060238

Lee et al., 2011

S.-J. Lee, B.-S. Huang, M. Ando, H.-C. Chiu, J.-H. Wang**Evidence of large scale repeating slip during the 2011 Tohoku-Oki earthquake**
Geophys. Res. Lett., 38 (2011), p. L19306

Lomnitz, 2004

C. Lomnitz**Major earthquakes of Chile: a historical survey, 1535–1960**
Seismol. Res. Lett., 75 (2004), pp. 368-378
CrossRefView Record in Scopus

Loveless et al., 2

J.P. Loveless, M.E. Pritchard, N. Kukowski**Testing mechanisms of subduction zone segmentation and seismogenesis with slip distributions from recent Andean earthquakes**
Tectonophysics, 495 (2010), pp. 15-33
ArticleDownload PDFView Record in Scopus

Meneses, 2014

E. Meneses**Análisis de la sismicidad y de parámetros de alerta temprana de terremotos para la zona de Iquique, norte de Chile**
Master's thesis
U. de Chile (2014)

Meng et al., 201

L. Meng, A. Inbal, J.P. Ampuero**A window into the complexity of the dynamic rupture of the 2011 Mw 9 Tohoku–Oki earthquake**
Geophys. Res. Lett., 38 (7) (2011)

Meng et al., 201

L. Meng, J.-P. Ampuero, Y. Luo, W. Wu, S. Ni**Mitigating artifacts in back-projection source imaging with implications on frequency-dependent properties of the Tohoku-Oki earthquake**
Earth Planets Space, 64 (2012), pp. 1101-1109
CrossRefView Record in Scopus

Meng et al., 201

L. Meng, J.P. Ampuero, A. Sladen, H. Rendon**High-resolution backprojection at regional distance: application to the Haiti M7.0 earthquake and comparisons with finite source studies**
J. Geophys. Res., 117 (2012), p. B04313

Meng et al., 201

L. Meng, R.M. Allen, J.P. Ampuero**Application of seismic array processing to earthquake early warning**
Bull. Seismol. Soc. Am., 104 (5) (2014), pp. 2553-2561
CrossRefView Record in Scopus

Meng et al., 201

L. Meng, J.-P. Ampuero, R. Bürgmann**The 2013 Okhotsk deep-focus earthquake: rupture beyond the metastable olivine wedge and thermally controlled rise time near the edge of a slab**
Geophys. Res. Lett., 41 (2014), 10.1002/2014GL059968

Métois et al., 201

M. Métois, A. Socquet, C. Vigny, D. Carrizo, S. Peyrat, A. Delorme, E. Maureira, M.-C.Valderas-Bermejo, I. Ortega**Revisiting the North Chile seismic gap segmentation using GPS-derived interseismic coupling**
Geophys. J. Int., 194 (2013), pp. 1283-1294
CrossRef

Nadeau and Joh

R.M. Nadeau, L.R. Johnson**Seismological studies at Parkfield VI: moment release rates and estimates of source parameters for small repeating earthquakes**
Bull. Seismol. Soc. Am., 88 (1998), pp. 790-814
View Record in Scopus

Nadeau and McE

R.M. Nadeau, T.V. McEvilly**Fault slip rates at depth from recurrence intervals of repeating microearthquakes**
Science, 285 (1999), pp. 718-721
CrossRefView Record in Scopus

Nadeau and McE

R.M. Nadeau, T.V. McEvilly**Periodic pulsing of characteristic microearthquakes on the San Andreas Fault**
Science, 303 (2004), pp. 220-222
CrossRefView Record in Scopus

Nakahara, 2008

H. Nakahara**Seismogram envelope inversion for high-frequency seismic energy radiation from moderate-to-large earthquakes**
Advances in Geophysics, vol. 40, Elsevier (2008), pp. 401-426
ArticleDownload PDFView Record in Scopus

Nielsen and Mad

S. Nielsen, R. Madariaga**On the self-healing fracture mode**
Bull. Seismol. Soc. Am., 93 (2003), pp. 2375-2388
CrossRefView Record in Scopus

Nishenko, 1985

S.P. Nishenko**Seismic potential for large and great interplate earthquakes along the Chilean and Southern Peruvian Margins of South America: a quantitative reappraisal**
J. Geophys. Res., 90 (1985), pp. 3589-3615
CrossRefView Record in Scopus

Noda and Lapus

H. Noda, N. Lapusta**Stable creeping fault segments can become destructive as a result of dynamic weakening**
Nature, 493 (2013), pp. 518-521
CrossRefView Record in Scopus

O'Hara et al., 20

K. O'Hara, K. Mizoguchi, T. Shimamoto, J.C. Hower**Experimental frictional heating of coal gouge at seismic slip rates: evidence for devolatilization and thermal pressurization of gouge fluids**
Tectonophysics, 424 (1) (2006), pp. 109-118
ArticleDownload PDFView Record in Scopus

Perfettini et al., 2

H. Perfettini, J.P. Avouac, J.C. Ruegg**Geodetic displacements and aftershocks following the 2001** Mw=8.4 **Peru earthquake: implications for the mechanics of the earthquake cycle along subduction zones**
J. Geophys. Res., 110 (2005), p. B09404

Peyrat et al., 201

S. Peyrat, R. Madariaga, E. Buforn, J. Campos, G. Asch, J.P. Vilotte**Kinematic rupture process of the 2007 Tocopilla earthquake and its main aftershocks from teleseismic and strong-motion data**
Geophys. J. Int., 182 (3) (2010), pp. 1411-1430
CrossRefView Record in Scopus

Ruiz et al., 2014

S. Ruiz, M. Metois, A. Fuenzalida, J. Ruiz, F. Leyton, R. Grandin, C. Vigny, R. Madariaga, J.Campos**Intense foreshocks and a slow slip event preceded the 2014 Iquique Mw 8.1 earthquake**
Science, 345 (6201) (2014), pp. 1165-1169
CrossRefView Record in Scopus

Schmidt et al., 2005

D.A. Schmidt, R. Bürgmann, R.M. Nadeau, M. d'Alessio**Distribution of aseismic slip rate on the Hayward fault inferred from seismic and geodetic data**
J. Geophys. Res., 110 (2005), p. B08406

Schurr et al., 2014

B. Schurr, G. Asch, S. Hainzl, J. Bedford, A. Hoechner, M. Palo, R. Wang, M. Moreno, M.Bartsch, Y. Zhang, O. Oncken, F. Tilmann, T. Dahm, P. Victor, S. Barrientos, J.-P. Vilotte**Gradual unlocking of plate boundary controlled initiation of the 2014 Iquique earthquake**
Nature, 512 (2014), pp. 299-302
CrossRefView Record in Scopus

Shirzaei et al., 2014

M. Shirzaei, R. Bürgmann, N. Uchida, Y. Hu, F. Pollitz, T. Matsuzawa**Seismic versus aseismic slip: probing mechanical properties of the northeast Japan subduction zone**
Earth Planet. Sci. Lett., 406 (2014), pp. 7-13
ArticleDownload PDFView Record in Scopus

Song and Simons, 2003
T.-R.A. Song, M. Simons**Large trench-parallel gravity variations predict seismogenic behavior in subduction zones**
Science, 301 (2003), pp. 630-633
CrossRefView Record in Scopus

Sulem and Famin, 2009
J. Sulem, V. Famin**Thermal decomposition of carbonates in fault zones: slip-weakening and temperature-limiting effects**
J. Geophys. Res., 114 (2009), p. B03309, 10.1029/2008JB006004

Templeton et al., 2008
D.C. Templeton, R.M. Nadeau, R. Bürgmann**Behavior of repeating earthquake sequences in Central California and the implications for subsurface fault creep**
Bull. Seismol. Soc. Am., 98 (2008), pp. 52-65
CrossRefView Record in Scopus

Uchida and Matsuzawa, 2013
N. Uchida, T. Matsuzawa**Pre- and postseismic slow slip surrounding the 2011 Tohoku-oki earthquake rupture**
Earth Planet. Sci. Lett., 374 (2013), pp. 81-91
ArticleDownload PDFView Record in Scopus

Uchida et al., 2004
N. Uchida, A. Hasegawa, T. Matsuzawa, T. Igarashi**Pre- and post-seismic slow slip on the plate boundary off Sanriku, NE Japan associated with three interplate earthquakes as estimated from small repeating earthquake data**
Tectonophysics, 385 (2004), pp. 1-15
ArticleDownload PDFView Record in Scopus

Vallée et al., 2008
M. Vallée, M. Landès, N.M. Shapiro, Y. Klinger**The 14 November 2001 Kokoxili (Tibet) earthquake: high-frequency seismic radiation originating from the transitions between sub-Rayleigh and supershear rupture velocity regimes**
J. Geophys. Res., Solid Earth (1978–2012), 113 (B7) (2008)

Wang and Bilek, 2011
K. Wang, S.L. Bilek**Do subducting seamounts generate or stop large earthquakes?**
Geology, 39 (2011), pp. 819-822
CrossRefView Record in Scopus

Yagi et al., 2014

Y. Yagi, R. Okuwaki, B. Enescu, S. Hirano, Y. Yamagami, S. Endo, T. Komoro**Rupture process of the 2014 Iquique Chile Earthquake in relation with the foreshock activity**
Geophys. Res. Lett., 41 (2014), 10.1002/2014GL060274

Yao et al., 2011

H. Yao, P. Gerstoft, P.M. Shearer, C. Mecklenbräuker**Compressive sensing of the Tohoku-Oki Mw 9.0 earthquake: frequency-dependent rupture modes**
Geophys. Res. Lett., 38 (2011), p. L20310, 10.1029/2011GL049223

$$\mathrm{Mw} = \tfrac{2}{3}\mathrm{Ml} + 1.56 \quad \text{if}\,\mathrm{Ml} \leq 4.41$$

$$\mathrm{Mw} = \mathrm{Ml} + 0.09 \quad \text{if} 4.41 < \mathrm{Ml} < 5.71$$